



Source-Dependent Optical Properties and Molecular Characteristics of Atmospheric Brown Carbon

Authors: Jinghao Zhai^{1,3}, Yin Zhang^{1,2}, Pengfei Liu⁴, Yujie Zhang^{1,2}, Antai Zhang^{1,2}, Yaling Zeng^{1,2}, Baohua Cai^{1,2}, Jingyi Zhang^{1,2}, Chunbo Xing^{1,2}, Honglong Yang⁵, Xiaofei Wang³, Jianhuai Ye^{1,2}, Chen Wang^{1,2}, Tzung-May Fu^{1,2}, Lei Zhu^{1,2}, Huizhong Shen^{1,2}, Shu Tao^{1,2}, Xin Yang^{1,2*}

¹*Shenzhen Key Laboratory of Precision Measurement and Early Warning Technology for Urban Environmental Health Risks, School of Environmental Science and Engineering, Southern University of Science and Technology, Shenzhen 518055, China*

²*Guangdong Provincial Observation and Research Station for Coastal Atmosphere and Climate of the Greater Bay Area, Shenzhen 518055, China*

³*Shanghai Key Laboratory of Atmospheric Particle Pollution and Prevention (LAP³), Department of Environmental Science and Engineering, Fudan University, Shanghai 200438, China*

⁴*School of Earth and Atmospheric Sciences, Georgia Institute of Technology, Atlanta, GA 30332, USA*

⁵*Shenzhen National Climate Observatory, Meteorological Bureau of Shenzhen Municipality, Shenzhen 518040, China*

*To whom correspondence should be addressed.

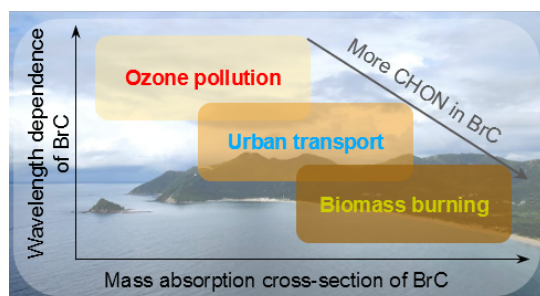
Correspondence to: Xin Yang

Email: yangx@sustech.edu.cn



ABSTRACT: Atmospheric brown carbon (BrC) can significantly affect Earth's radiation budget by its wavelength-dependent absorption in the ultraviolet (UV)-visible range. BrC consists of a wide variety of organics with different optical properties, making accurate climate modeling essential for understanding its radiative impact. Here, we conducted a field campaign during the summer in Shenzhen, China, to investigate the optical properties and molecular characteristics of BrC from diverse particle sources using both online and offline measurements. Different sources of BrC, including those from secondary production associated with ozone pollution, urban transportation, and biomass burning, were identified through meteorological data and particle chemical compositions. The results show that the mass absorption cross-section (MAC) of BrC varied across sources, with BrC from biomass combustion exhibiting the highest MAC at 370 nm ($3.42 \pm 0.41 \text{ m}^2/\text{g}$) and secondary BrC associated with ozone pollution showing the lowest ($1.25 \pm 0.56 \text{ m}^2/\text{g}$). Nevertheless, secondary BrC exhibited the highest absorption Ångström exponent (AAE) while the BrC from biomass burning had the lowest AAE. Molecular analysis revealed that species in the CHON family from biomass burning demonstrated the strongest light absorption. Our results provide valuable insights for quantifying the source-specific optical properties of BrC, enhancing the accuracy of climate models.

Graphical abstract





42 1 INTRODUCTION

43 Atmospheric light-absorbing organic aerosols, known as brown carbon (BrC), are important
44 contributors to the global radiation absorption of atmospheric aerosols, alongside black carbon
45 (BC). The absorption properties of BrC are wavelength-dependent, with relatively weak absorption
46 in the mid- and long-visible wavelengths and a pronounced increase in absorption toward the short-
47 visible and near-ultraviolet (UV) wavelengths (Sun et al., 2007;Laskin et al., 2015). Atmospheric
48 BrC is primarily generated from the combustion of biomass and biofuels, as these processes
49 typically occur under relatively low-temperature, fuel-rich conditions, which promote the
50 formation of organics (Saleh et al., 2014;Chen and Bond, 2010). Additionally, secondary reactions
51 in the atmosphere also play a significant role in the production of BrC (Laskin et al., 2015;Moise
52 et al., 2015). It has been observed that BrC can be formed in secondary organic aerosols (SOA)
53 through the nitration of volatile organic compound (VOC) precursors (Zhong and Jang,
54 2011;Lambe et al., 2013;Updyke et al., 2012;Haynes et al., 2019), aqueous-phase reactions of
55 ammonia or amino acids with carbonyl-containing SOA (Updyke et al., 2012;Flores et al.,
56 2014;Zarzana et al., 2012), and bond-forming reactions among SOA constituents that generate
57 dimers and larger oligomers (Shapiro et al., 2009;Bones et al., 2010;Chang and Thompson, 2010).
58 Unlike BC, which exhibits relatively uniform physicochemical properties, BrC comprises a broad
59 spectrum of light-absorbing organic species, resulting in large variability in its optical properties
60 (Updyke et al., 2012;Saleh et al., 2018). To accurately assess the radiative impacts of BrC, its
61 diverse properties must be effectively represented in climate models.

62 Aerosol light absorption can be quantified using the mass absorption cross-section (MAC), a
63 key parameter that links radiative transfer to aerosol mass in climate models (Bond and Bergstrom,
64 2006). MAC can be calculated from measurements of aerosol light absorption coefficient and mass
65 concentration. The absorption Ångström exponent (AAE) describes the wavelength dependence
66 of aerosol light absorption. For BC aerosols, AAE values are typically close to 1 (Bond and
67 Bergstrom, 2006). In contrast, BrC shows substantial variability in wavelength dependence, with
68 AAE values ranging from 2 to as high as 11 (Laskin et al., 2015). The optical properties of BrC



69 are highly source-dependent (Saleh et al., 2014;Kumar et al., 2018). Moreover, BrC absorption
 70 evolves dynamically during atmospheric aging through processes like photobleaching or photo-
 71 enhancement, leading to uncertainties in the quantification of the radiative effects of atmospheric
 72 aerosols (Wong et al., 2017;Sumlin et al., 2017;Li et al., 2020).

73 The measurement of the optical properties of BrC is crucial for accurately determining its role
 74 in global radiation balance. In filter-based offline analysis, the optical properties of a bulk film can
 75 be measured using an ultraviolet-visible (UV-vis) spectrometer (Zhong and Jang, 2011). However,
 76 the varying solubility of BrC in different solvents can introduce uncertainties in these
 77 measurements (Shetty et al., 2019). To address this issue, combining sequential solvent extraction
 78 with online optical measurements provides a more comprehensive understanding of the relative
 79 abundance of BrC classes (Kumar et al., 2018;Saleh et al., 2014). Nevertheless, the optical
 80 properties of BrC retrieved from online measurements can be subject to biases due to the
 81 limitations of the techniques employed. For example, transmission measurements through aerosol-
 82 laden filters have been used to quantify aerosol absorption properties (Petzold et al., 2005;Bond
 83 and Bergstrom, 2006). These approaches usually assume that aerosol particles retain their
 84 morphology upon adhering to the filters, potentially leading to uncertainties in the interpretation
 85 of filter absorption data (Subramanian et al., 2007). Various online approaches have been
 86 developed to directly measure the absorption, scattering, and extinction coefficients of aerosols,
 87 either independently or in combination. Cavity-based techniques offer highly sensitive and
 88 accurate measurements of the overall extinction coefficient (Riziq et al., 2007;Massoli et al., 2010).
 89 An integrating nephelometer enables the independent measurement of the scattering coefficient
 90 (Anderson and Ogren, 1998;Bond et al., 2009). Photoacoustic instruments are widely recognized
 91 for providing accurate absorption measurements (Arnott et al., 1998;Lewis et al., 2008). Studies
 92 comparing photoacoustic and filter-based methods indicate that filter-based techniques often
 93 overestimate absorption, although the AAE derived from both methods generally aligns more
 94 closely (Al Fischer and Smith, 2018;Saleh et al., 2014).



95 The complex chemical composition of BrC leads to significant variability in its optical
96 properties. The molecular characteristics of BrC components vary based on their sources, making
97 specific molecular information valuable for source attribution. Studies have shown that the
98 molecules responsible for BrC absorption in biomass burning aerosols tend to be large and highly
99 unsaturated (Sun et al., 2007). Nitrophenols, nitrobenzene, and their derivatives are commonly
100 identified as BrC molecules, either directly emitted from biomass burning or formed through
101 atmospheric reactions involving combustion products, nitrogen oxides, or nitrous acid (Li et al.,
102 2014; Chen et al., 2011; Desyaterik et al., 2013). Amines, another group of nitrogen-containing
103 compounds, are often detected in BrC, where they frequently serve as reactants in the formation
104 of SOA (Nozière et al., 2009). High-resolution mass spectrometry (HRMS) has been widely used
105 for offline characterization of BrC to obtain detailed molecular-level information. To improve
106 detection accuracy, BrC components are often separated using chromatography before MS
107 analysis, allowing for more precise molecular identification (Claeys et al., 2012; Zhang et al.,
108 2013; Desyaterik et al., 2013). To fully understand how the chemical variability of BrC influences
109 atmospheric radiation, it is crucial to conduct detailed chemical analyses of BrC and incorporate
110 the updated BrC classifications into the climate models.

111 Previous studies on BrC have mostly been based on laboratory simulations of typical sources,
112 with limited direct field measurements of physicochemical properties of BrC across multiple
113 sources, partly due to the challenges in distinguishing BrC from different sources under complex
114 ambient conditions. In this study, we conducted a field campaign during the summer of 2022 at
115 Xichong site (22.48°N, 114.56°E), located on the Dapeng Peninsula of Shenzhen, China. Particle
116 optical properties and chemical compositions were measured both online and offline. Different
117 sources of BrC were identified through meteorological data and the chemical compositions of
118 particles. The optical properties of BrC from different sources were evaluated and compared,
119 supported by molecular characterizations. Our study provides direct observational evidence of
120 varying BrC sources with different optical properties in the ambient, contributing to a deeper
121 understanding of BrC's radiative effects in climate models.



122 2 METHODS

123 2.1 Field Measurements

124 Field measurements were conducted at Xichong site (22.48°N, 114.56°E, Figure S1) on the Dapeng
 125 Peninsula in Shenzhen, China, from August to September 2022. Located about 60 km from the
 126 city center, Xichong site is surrounded by the sea and distant from urban areas and industrial
 127 sources, with over 90% forest coverage. Due to minimal local anthropogenic interference, Xichong
 128 site serves as a regional atmospheric background station in South China.

129 During the field campaign, an aethalometer (AE31, Magee Scientific, USA) operating at seven
 130 wavelengths (370, 470, 520, 590, 660, 880, and 950 nm) and a photoacoustic extinctions (PAX,
 131 Droplet Measurement Techniques, USA) measuring at 532 nm, were utilized to detect the online
 132 optical properties of particles. A Monitor for Aerosols and Gases in Ambient air (MARGA,
 133 Metrohm-Applikon, Netherlands) was conducted to detect the online water-soluble ion
 134 concentration (NH_4^+ , Na^+ , K^+ , Ca^{2+} , Mg^{2+} , SO_4^{2-} , NO_3^- , Cl^-). Detailed information regarding the
 135 instrumentation and measurement uncertainties of the aethalometer is provided in the Supporting
 136 Information (SI, Text S1). In this study, the time resolution of all online data was standardized to
 137 1 h. Offline filter sampling was also carried out simultaneously during the field campaign. A high-
 138 volume sampler (XT1025, XTrust Analytical Instruments, China) with a flowrate of $1\text{ m}^3/\text{min}$ was
 139 used to collect $\text{PM}_{2.5}$ samples on the pre-baked quartz filters with sampling period of 24 h for each
 140 filter. Details on the filter pretreatment procedures are available in the SI (Text S2). The filters
 141 were further analyzed to measure the BrC mass, optical properties, and molecular characteristics.

142 Other measurements including the mass concentration of $\text{PM}_{2.5}$, O_3 , and the meteorological
 143 factors (temperature, relative humidity, wind speed, and wind direction), were conducted at the
 144 sampling site. The HYSPLIT-4 (Hybrid Single-Particle Lagrangian Integrated Trajectory) model
 145 developed by the ARL (Air Resources Laboratory) of the NOAA (National Oceanic and
 146 Atmospheric Administration, USA) was employed to compute 24 h air mass back trajectories at a
 147 50 m arrival height.



148 2.2 Mass absorption cross-section of BrC

149 The mass absorption cross-section (MAC, m²/g) of BrC can be calculated according to the
 150 following equation:

$$151 \quad \text{MAC}(\lambda) = \frac{b_{\text{abs,BrC}}(\lambda)}{[\text{BrC}]} \quad (1)$$

152 where $b_{\text{abs,BrC}}(\lambda)$ is the light absorption coefficient (Mm⁻¹) of BrC at a given wavelength λ ,
 153 derived by subtracting the corresponding absorption coefficient of BC from the total particle
 154 absorption coefficient. Here, we used both online and offline methods to calculate the MAC of
 155 BrC.

156 Previous studies have reported that the b_{abs} estimated from the aethalometer is generally larger
 157 than that measured by the PAX, likely due to artifacts associated with organic matter loading on
 158 the filter (Lack et al., 2008;Cappa et al., 2008;Saleh et al., 2014). In this study, the correlation
 159 between the b_{abs} derived from the aethalometer ($b_{\text{abs,520}}$) and the PAX ($b_{\text{abs,532}}$) is shown in
 160 Figure S2. The aethalometer-derived b_{abs} were scaled by a factor of 2 across all wavelengths for
 161 subsequent MAC calculations. We consider the light absorption coefficient at a wavelength of 880
 162 nm detected by the aethalometer to be primarily attributed to BC, with minimal contribution from
 163 BrC absorption (Laskin et al., 2015). Based on the fact that BC has minimal wavelength
 164 dependence, with an AAE of ~1 (Bond and Bergstrom, 2006), the BC absorption coefficient at
 165 wavelength λ , $b_{\text{abs,BC}}(\lambda)$, is given by:

$$166 \quad b_{\text{abs,BC}}(\lambda) = b_{\text{abs,BC}}(880) \times \left(\frac{\lambda}{880}\right)^{-1} \quad (2)$$

167 And thus the $b_{\text{abs,BrC}}(\lambda)$ is calculated by:

$$168 \quad b_{\text{abs,BrC}}(\lambda) = b_{\text{abs}}(\lambda) - b_{\text{abs,BC}}(\lambda) \quad (3)$$

169 The light absorption coefficients of the aethalometer were not directly measured but were
 170 converted and corrected (Text S1). In this study, we focus on wavelengths of 370 nm and 550 nm
 171 for all the optical measurements, representing the high light absorption band and mid-visible band



of BrC, respectively, to facilitate comparisons with results from other studies. Thus, the absorption coefficient at 520 nm wavelength detected by the aethalometer was converted to 550 nm using the following equations:

$$b_{\text{abs}}(550) = b_{\text{abs}}(520) \times \left(\frac{550}{520}\right)^{-AAE_{370-550}} \quad (4)$$

$$AAE_{370-550} = -\frac{\ln[b_{\text{abs}}(370)] - \ln[b_{\text{abs}}(550)]}{\ln(370) - \ln(550)} \quad (5)$$

In equation (1), [BrC] is the mass concentration of BrC. Since BrC is fundamentally an optical concept, the optical-equivalent mass of BrC can be determined according to the absorption coefficient of BrC by assuming its MAC. Currently, there is no unified method for the direct measurement of BrC mass. Commonly used methods for characterizing BrC include thermal desorption and dissolution methods for characterization of BrC mass, although both come with inherent uncertainties. The thermal desorption method quantifies BrC mass by heating the volatile OC of the particle, taking advantage of the lower volatilization point of BrC than BC (Massabò et al., 2016; Olson et al., 2015; Pani et al., 2021). However, it may also include some non-absorbing OC and may induce pyrolysis during the heating process, which brings further uncertainties into the measurement. The dissolution method measures the BrC mass after extraction in the solvent (water, methanol, acetone, etc.) (Rathod et al., 2024). Nevertheless, some BrC may not be soluble, which carries uncertainties to the dissolution method.

In this study, we used both thermal desorption and dissolution methods to measure the [BrC]. For the thermal desorption method, the BrC mass was measured using an organic carbon/elemental carbon analyzer (OC/EC analyzer, DRI 2015, Magee Scientific, USA) based on the filter samples. Detailed information on the OC/EC analyzer mechanism is provided in the SI (Text S3). The temperature-separated carbon fractions from aerosol filter deposits were quantified for the mass concentration of OC that evaporated up to 580°C ([OC_T]), which was taken as a representative of the BrC mass concentration to calculate the MAC.



During the campaign, the optical measurement function of the OC/EC analyzer was malfunctioning. The $b_{\text{abs,BrC}}$ values were based on online data from the aethalometer ($b_{\text{abs,AE31}}$) with one data point per hour, whereas the $[\text{OC}_T]$ values were derived from offline filter sampling with one data point every 24 hours. To align the temporal resolution of the data, we used $[\text{OC}_T]$ relative to the total particulate mass ($\text{PM}_{\text{filter}}$) on each filter (every 24 hours) as a fixed ratio. This ratio was then applied to the hourly $\text{PM}_{2.5}$ mass concentration ($[\text{PM}_{2.5}]$) over the corresponding 24-hour period, yielding the calculated hourly BrC mass concentration as given by equation (3). There might be limitations arising from the fixed BrC mass ratio ($\frac{[\text{OC}_T]}{[\text{PM}_{\text{filter}}]}$) used to calculate the MAC over 24 hours, as the time resolution differs from the hourly $b_{\text{abs,AE31}}$. However, we believe that the quantification of BrC mass in this study does rely on the offline filter-based analysis. The time resolution of the online $\text{MAC}_{\text{BrC},\lambda}$ in this study is one hour.

$$\text{MAC}_{\text{BrC},\lambda} = \frac{b_{\text{abs,AE31}}(\lambda)}{\frac{[\text{OC}_T]}{[\text{PM}_{\text{filter}}]} \times [\text{PM}_{2.5}]} \quad (6)$$

Meanwhile, we measured the mass concentration and light absorption of water-soluble organic carbon (WSOC). The solubility of BrC varies across different solvents. However, in this study, the mass concentration of WSOC ($[\text{WSOC}]$) was chosen for the calculation of MAC, and BrC dissolved in other solvents was not further discussed. The mass concentration of WSOC in the collected filter samples was measured using a total organic carbon analyzer (TOC analyzer, N/C 3100, Analytik Jena, Germany). We further compared the $[\text{OC}_T]$ detected by the thermal desorption method and the $[\text{WSOC}]$ measured by the dissolution method (Figure S3), which showed good correlation ($r^2=0.844$) while the $[\text{OC}_T]$ was more than twice of the $[\text{WSOC}]$.

The light absorption of WSOC was further measured using an ultraviolet- visible (UV-vis) spectrometer (T2600, York Instrument, China) within the wavelength ranging from 190 to 1100 nm. The WSOC light absorption was then converted into light absorption coefficients ($b_{\text{abs,WSOC}}$), as given by equation (4):

$$b_{\text{abs,WSOC}}(\lambda) = \ln(10) \times (A_\lambda - A_{880}) \times \frac{V_l}{V_a \times L} \quad (7)$$



where A_{880} is the systematic baseline drift, V_l (m^3) is the volume of water (30 mL) used for extraction, V_a (m^3) is the volume of the sampled air, and L (m) is the optical path length of the quartz cuvette (1 cm) in the UV-vis spectrometer. The filter-based offline $\text{MAC}_{\text{WSOC},\lambda}$ is calculated according to:

$$\text{MAC}_{\text{WSOC},\lambda} = \frac{b_{\text{abs,WSOC}}(\lambda)}{[\text{wsoc}]} \quad (8)$$

2.3 Chemical molecular analysis

A high-performance liquid chromatography (HPLC) equipped with a photodiode array (PDA, G7117C, Agilent, USA) detector and a high-resolution mass spectrometer system (HRMS, G6545A, Agilent, USA) was utilized to identify the molecular composition, determine the relative abundance, and measure the corresponding light absorption of BrC. The HPLC was equipped with a C18 column (EC-C18, 3×150 mm, $2.7 \mu\text{m}$ particles, Agilent, USA), using mobile phases of 0.1% formic acid-water (A, HPLC grade) and 0.1% formic acid-acetonitrile (B, HPLC grade). Gradient elution for each sample was performed with the A-B mixture as: 0~1 min hold at 95% A, 1~20 min linear decreased to 5% A, 20~27 min hold at 5% A, and then 27~30 min hold at 95% A. The HRMS was set with a soft electrospray ionization source (ESI) in full scan, operating in both positive and negative ion modes. Raw data from mass spectrometry were processed using MassHunter Qualitative Analysis (v10.0). Molecule concentrations were semi-quantified based on the intensity from mass spectrometry (Kruve, 2019; Zhang et al., 2023).

The absorbance of the PDA at 370 nm was selected as the intensity of light absorption of BrC (Hecobian et al., 2010; Wen et al., 2021). Using a peak extraction algorithm in MassHunter Qualitative Analysis, approximately 20 absorption peaks per sample were identified. The absorption intensity at a specific retention time was determined by subtracting the blank absorption from the sample absorption. Peaks were grouped by overlapping retention times, with molecules in each group recorded along with their absorbance detected by the PDA. We employed a partial least squares regression (PLSR) model to attribute individual molecular absorbance (Text S4),



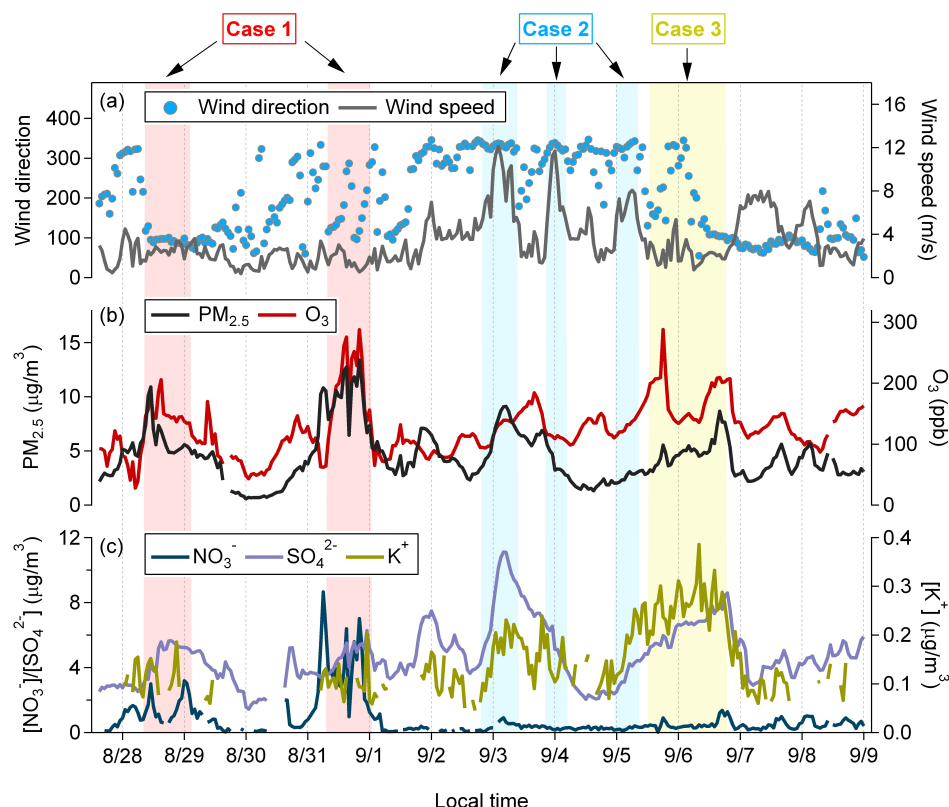
clarifying the relationship between absorbing molecules and the absorbance of individual peaks (Zhang et al., 2023).

3 RESULTS AND DISCUSSION

3.1 Light absorption of BrC from different sources

During our sampling period, wind at the Xichong site predominantly came from two directions: northwest and northeast (Figure 1a, Figure S4). Air masses from the northwest primarily originated from inland areas of the peninsula, while those from the northeast were from the sea (Figure S1). High ozone levels were observed at times, mainly during the daytime, and were associated with relatively high nitrate concentrations (Figures 1b & 1c). Additionally, water-soluble potassium, as a marker for biomass-combusted aerosols (Zhai et al., 2015), also exhibited a time of elevated levels during our observation (Figure 1c). Based on distinct meteorological and pollutant concentration characteristics, we selected three typical cases for detailed analysis of their optical properties. The selection criteria for each case were as follows: Case 1, the ozone case, with 1) the concentration of $O_3 > 100$ ppb, 2) the concentration of $[NO_3^-] > 0.6 \mu g/m^3$, 3) wind speed < 3 m/s, and 4) consecutive duration > 6 h (red shading in Figure 1); Case 2, the transport case with 1) wind direction $> 270^\circ$, 2) wind speed > 4 m/s, and 3) consecutive duration > 6 h (blue shading in Figure 1); and Case 3, the combustion case, with 1) the concentration of $[K^+] > 0.2 \mu g/m^3$, and 2) consecutive duration > 6 h (yellow shading in Figure 1).

Meanwhile, the HYSPLIT 24-h air mass backward trajectories indicate that during Case 1, air masses predominantly originated from areas close to the sampling site. Combined with low wind speeds (< 3 m/s), meteorological conditions limited atmospheric dispersion, promoting ozone accumulation and secondary pollutant formation (Figure S5). In Case 2, the air mass trajectories were from the inland region, with strong wind speeds that facilitated the transport of pollutants to the sampling site. For Case 3, the air mass trajectories also originated from the interior region but were associated with lower wind speeds than in Case 2.



271

272 **Figure 1.** Time series of wind direction and wind speed at the sampling site (a), the concentration
 273 of $\text{PM}_{2.5}$ and O_3 (b), and chemical composition detected by the MARGA (NO_3^- , SO_4^{2-} , and K^+ , d).
 274 The colored shadows denote the sampling time for the studied cases (red shading for ozone Case
 275 1, blue shading for transport Case 2, and yellow shading for combustion Case 3).

276 Polar plots of wind direction, wind speed, and $\text{MAC}_{\text{BrC},370}$ were further analyzed for Case 1–3
 277 (Figure 2). In Case 1, the average wind speed was 2.06 m/s, with pollution mainly from local
 278 sources (Figure 2a). During Case 1, the average $\text{PM}_{2.5}$ concentration was $8.05 \pm 2.67 \mu\text{g}/\text{m}^3$, and
 279 the average $\text{MAC}_{\text{BrC},370}$ was $1.25 \pm 0.56 \text{ m}^2/\text{g}$ (Figure 2d). For Case 2, the wind primarily came
 280 from the northwest, passing over the peninsula, with an average wind speed of 7.81 m/s (Figure
 281 2b). The average $\text{PM}_{2.5}$ concentration and $\text{MAC}_{\text{BrC},370}$ for Case 2 were $4.87 \pm 2.36 \mu\text{g}/\text{m}^3$ and 2.68
 282 $\pm 0.30 \text{ m}^2/\text{g}$, respectively. In Case 3, the wind speed averaged 2.19 m/s, with erratic wind directions



(Figure 2c). The average $\text{PM}_{2.5}$ concentration and $\text{MAC}_{\text{BrC},370}$ for Case 3 were $5.05 \pm 1.32 \mu\text{g}/\text{m}^3$ and $3.42 \pm 0.41 \text{ m}^2/\text{g}$, respectively.

Among the three cases, although the average $\text{PM}_{2.5}$ concentration in Case 1 was the highest, its $\text{MAC}_{\text{BrC},370}$ was the lowest, indicating that the light-absorbing ability of BrC in this high-ozone scenario was relatively weak. The low wind speed in Case 1 limited the influx of transported pollutants. High concentrations of ozone and $[\text{NO}_3^-]$ indicated that the aerosols in Case 1 were primarily secondary and highly aged. However, Case 3, characterized by a high concentration of potassium and identified as a plume from combustion sources, had the highest $\text{MAC}_{\text{BrC},370}$ in our observations, indicating the strongest light-absorbing ability of combusted BrC among the cases.

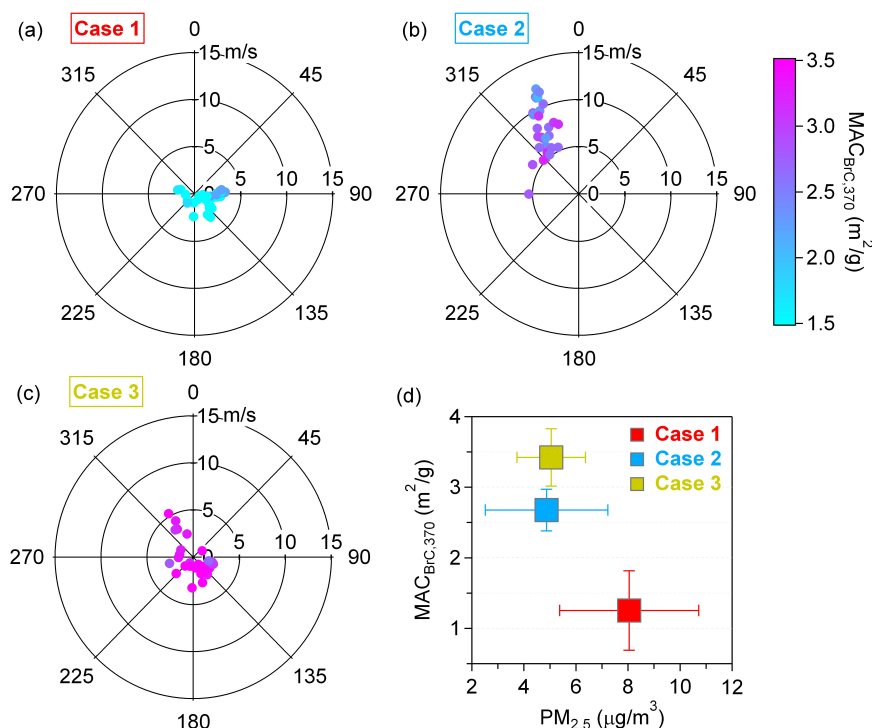


Figure 2. (a–c) Polar plots and $\text{MAC}_{\text{BrC},370}$ values for Case 1–3. The radius and color represent the $\text{MAC}_{\text{BrC},370}$ values in the downwind direction at specific wind speeds. The color scale denotes the values of $\text{MAC}_{\text{BrC},370}$. (d) The mean $\text{MAC}_{\text{BrC},370}$ values and mean $\text{PM}_{2.5}$ values for Case 1–3. Error



bars denote a standard deviation.

3.2 Effects of different aerosol sources on the MAC

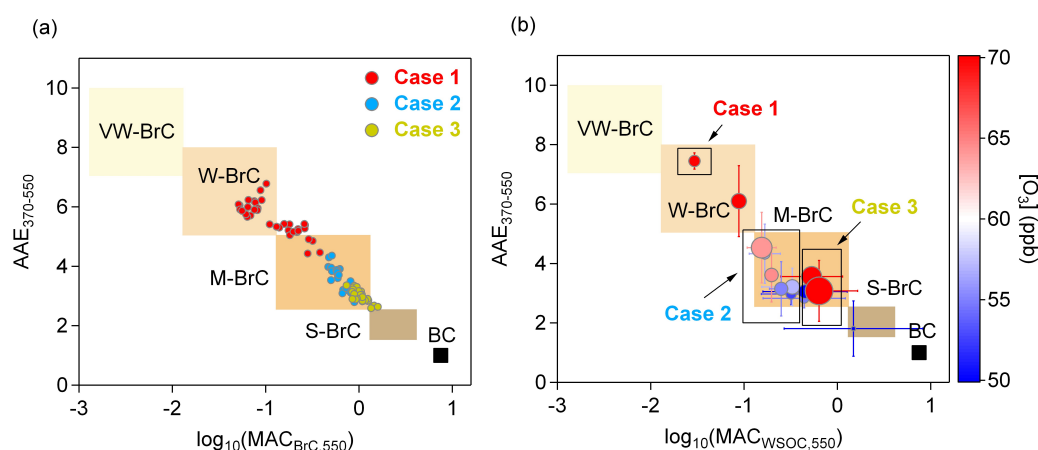
By compiling BrC light-absorption measurements reported in 20 studies, Saleh et al. classified BrC into four classes (Saleh, 2020), each with characteristic $MAC_{BrC,550}$ and AAE values: very weakly absorbing (VW-BrC, $MAC_{BrC,550}$ of 1.3×10^{-3} – 1.3×10^{-2} , AAE of 7–10), weakly absorbing (W-BrC, $MAC_{BrC,550}$ of 1.3×10^{-2} –0.13, AAE of 5–8), moderately absorbing (M-BrC, $MAC_{BrC,550}$ of 0.13–1.3, AAE of 2.5–5), and strongly absorbing (S-BrC, $MAC_{BrC,550} > 1.3$, AAE of 1.5–2.5). The optical properties defining these BrC classes are expected to be associated with their corresponding physicochemical properties, such as molecular size, volatility, and solubility. In this study, the AAE values for both online measurements of BrC and filter-based offline measurements of WSOC were calculated in the wavelength range of 370 nm to 550 nm, referred to as $AAE_{370-550}$.

For online measurements of BrC, the optical results show an approximately linear correlation. In Case 1, results fall into both the W-BrC and M-BrC categories, whereas results for Case 2 and Case 3 fall primarily into the M-BrC category (Figure 3a). In Case 1, where the ozone concentration is high, BrC shows weaker light-absorbing ability and stronger wavelength dependence compared to Cases 2 & 3. BrC in Case 3 exhibits a high light-absorbing ability with low wavelength dependence. For Case 2, a portion of the optical results overlaps with those from Case 3, possibly due to the transported air mass originating from a similar source as in Case 3.

For the filter-based offline measurements of WSOC, the trend of $AAE_{370-550}$ and $MAC_{WSOC,550}$ is consistent with the online results, showing an inverse correlation (Figure 3b). The sample in Case 1 shows the highest wavelength dependence and the lowest light-absorbing ability of WSOC. It's worth noting that although the ozone concentration was also high during Case 3, its optical results did not exhibit the same high wavelength dependence as observed in Case 1. The possible reason could be that primary WSOC produced by combustion has stronger light absorption, which dominated the optical behavior of WSOC during Case 3.



321 Saleh et al. suggested that VW-BrC primarily originates from secondary BrC, W-BrC mainly
 322 comes from smoldering BrC, and M-BrC is mainly associated with high-temperature BrC (Saleh,
 323 2020). However, in our observations, we found that Case 1, which we consider to be dominated
 324 by secondary BrC, still falls within the W-BrC or even M-BrC regions for both online airborne
 325 measurements and filter-based offline analysis. Possible reasons could be: 1) Unlike laboratory
 326 studies, field environments have greater diversity and uncertainty in BrC sources, and 2)
 327 differences in measurement methods may lead to variations in the results (Bond and Bergstrom,
 328 2006;Saleh, 2020). Although the results for Case 2 fall solely within the S-BrC category, we
 329 believe that particles during this period are transported from inland urban areas, where the sources
 330 are more complex, including contributions from traffic emissions, industrial combustion,
 331 secondary sources, etc.



332

333 **Figure 3.** Optical-based BrC classification scheme (Saleh, 2020) in the $\log_{10}(\text{MAC}_{550})$ vs. $\text{AAE}_{370-550}$
 334 space for (a) BrC and (b) WSOC. The shaded areas represent very weakly absorbing BrC (VW-
 335 BrC), weakly absorbing BrC (W-BrC), moderately absorbing BrC (M-BrC), and strongly
 336 absorbing BrC (S-BrC). BC is also shown for reference (Bond and Bergstrom, 2006). The scatters
 337 in (a) correspond to the online results of Case 1–3. The scatters in (b) correspond to the filter-based
 338 results during the sampling period with each scatter representing a filter in 24 h sampling duration.



339 The color scale in (b) denotes the ozone concentration in ppb. The size of scatters in (b) denotes
 340 the concentration of K^+ detected by the MARGAR. Error bars denote the standard deviation of the
 341 results for three repeated experiments.

342 **3.3 Chemical characterization of BrC molecules**

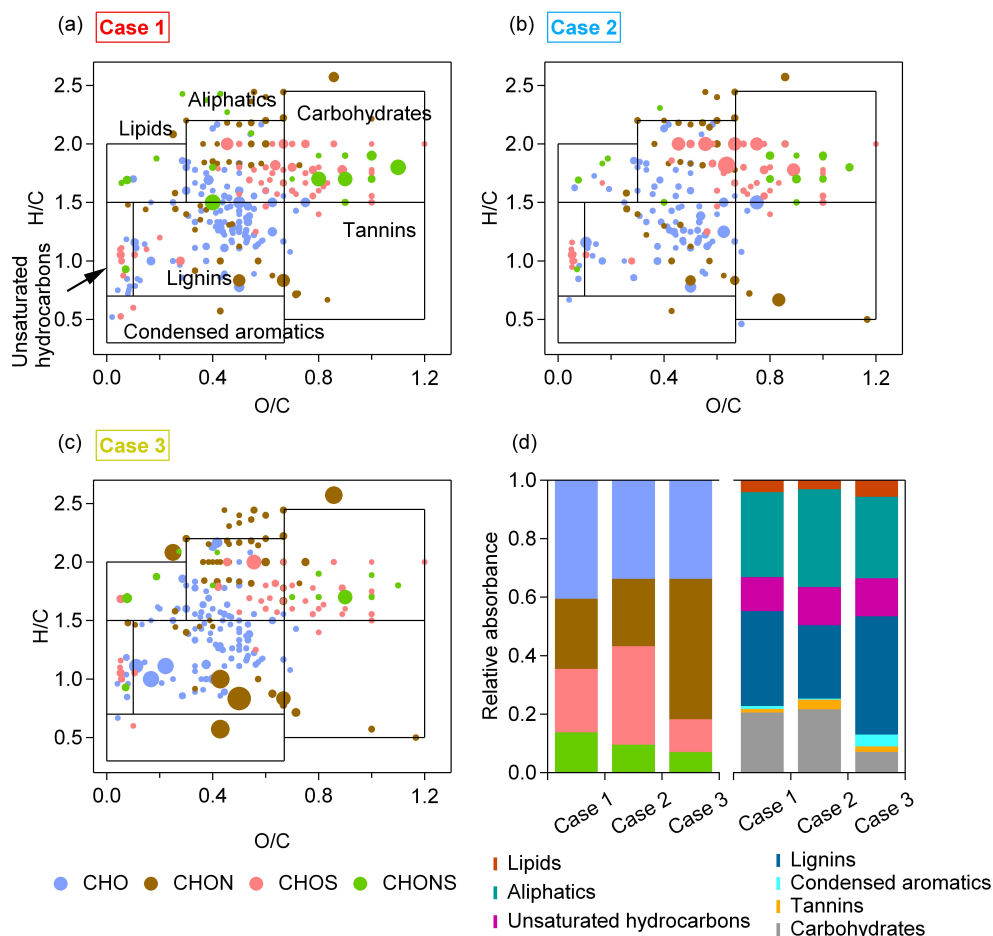
343 The water-soluble organic carbon (WSOC) species were ionized using ESI⁺ and ESI⁻ ionization
 344 modes to detect the organic compounds. The identified molecules were categorized into groups
 345 based on atom composition: CHO, CHON, CHOS, and CHONS. The van Krevelen (VK) diagram
 346 is a widely used graphical method that plots H/C ratios against O/C ratios in molecular formulas
 347 to qualitatively identify the major chemical species in WSOC (Kim et al., 2003). In this study, the
 348 VK space is divided into seven regions based on previous studies: (1) lipid-like (O/C = 0–0.3, H/C
 349 = 1.5–2.0), (2) aliphatic/protein-like (O/C = 0.3–0.67, H/C = 1.5–2.2), (3) carbohydrate-like (O/C
 350 = 0.67–1.2, H/C = 1.5–2.4), (4) unsaturated hydrocarbons (O/C = 0–0.1, H/C = 0.7–1.5), (5)
 351 lignins/carboxylic-rich alicyclic-molecule-like (CRAM) (O/C = 0.1–0.67, H/C = 0.7–1.5), (6)
 352 tannin-like (O/C = 0.67–1.2, H/C = 0.5–1.5), and (7) condensed aromatics (O/C = 0–0.67, H/C =
 353 0.2–0.7) (Feng et al., 2016; Ohno et al., 2010; Zeng et al., 2024). The sizes of scatters in Figure 4
 354 are proportional to the absorbance.

355 In Case 1, CHO compounds, which account for 36.5% of the absorbance, are the most abundant
 356 form of BrC. These CHO compounds likely contain carboxyl or hydroxyl functional groups and
 357 have been widely found in WSOC and cloud water (Bianco et al., 2018; Kourtchev et al., 2016).
 358 Secondary CHO compounds, including typical dimers of α -pinene and diterpenoid derivatives,
 359 have also been detected in previous studies (Kourtchev et al., 2014; Kristensen et al., 2014; Gómez-
 360 González et al., 2012). The CHOS group in Case 2 contributes the highest relative absorbance
 361 (29.5%). The CHOS compounds are considered to contain long aliphatic carbon chains with low
 362 aromaticity and are typically derived from anthropogenic emissions, such as diesel vehicles (Tao
 363 et al., 2014), coal combustions (Song et al., 2019), and vessels (Cui et al., 2019). The CHON group
 364 in Case 3 exhibits the highest relative absorbance (43.2%). It's worth noting that, although CHON



365 is not the most abundant group in terms of molecular abundance, its relative absorbance is the
366 highest, suggesting that CHON compounds have a strong molecular absorption capacity. The
367 CHON compounds have been found to be mainly derived from biomass burning species, such as
368 nitrophenols, nitrocatechols, nitroguaiacols, etc. (Kourtchev et al., 2015; Zhang et al., 2013; Song
369 et al., 2018). We further conducted a correlation analysis between the relative absorbance of
370 CHON and the MAC of WSOC throughout the whole sampling period, finding that as the relative
371 absorbance of CHON increases, the MAC of BrC also becomes larger (Figure S7). The
372 measurement of chemical molecules provides support for the results corresponding to our optical
373 observations in different cases.

374 In the VK diagram, aliphatics, lignins, and carbohydrates dominate in all three cases. In Case 3,
375 WSOC shows a higher proportion of absorbance from lignins, which are commonly attributed to
376 biomolecules and biomass burning species (Kitanovski et al., 2014). The differences in the
377 chemical molecular compositions of BrC across the different cases during our observations led to
378 variations in the light absorption of organic matter.



379

380 **Figure 4.** Sources of WSOC formula categories. (a–c) Van Krevelen plots for Case 1–3. Different
 381 formula categories are color coded. The sizes of scatters are proportional to the absorbance. The
 382 boxes indicate the classifications of various chemical species. (d) Relative absorbance of different
 383 formula categories (CHO, CHON, CHOS, and CHONS), and of different chemical species (lipids,
 384 aliphatics, unsaturated hydrocarbons, lignins, condensed aromatics, tannins, and carbohydrates).

385 4 CONCLUSIONS

386 The diverse chemical composition of atmospheric light-absorbing organics leads to distinct optical
 387 properties for BrC from different sources. However, studies on the optical properties of multi-



388 source atmospheric BrC, particularly those based on field observations, remain limited. The main
389 challenge arises from the complex and variable ambient conditions, which complicate the accurate
390 identification of BrC from different sources. In this study, a sampling site located away from urban
391 areas was selected, providing a more favorable environment for distinguishing BrC from primary
392 and secondary sources. Through field measurements, we independently identified various BrC
393 sources, including secondary BrC from ozone oxidation, primary BrC transported from urban
394 sources, and typical combustion-derived BrC. We found that the MAC of BrC varied by source,
395 with secondary BrC from ozone pollution being the least absorbing but exhibiting the highest AAE,
396 while BrC from biomass combustion was the most absorbing with the lowest AAE.

397 A key challenge in representing BrC absorption in climate models is its significant variability
398 in light absorption capacity. The representation of BrC absorption in climate models could be
399 improved by differentiating BrC sources or categorizing BrC into distinct optical ranges. Our direct
400 field measurements contribute to a better understanding of the optical properties of multi-source
401 BrC.

402



403 **Data availability.** Data used to produce the plots within this work are available in Zenodo
404 (<https://zenodo.org/records/14780067>).

405 **Author contributions.** JZ, XY, and PL designed the study. JZ and YZ analyzed the data. AZ and
406 YLZ performed the chemical molecular detections. JZ wrote the manuscript. All co-authors
407 contributed to discussions and suggestions in finalizing the manuscript.

408 **Competing interests.** The contact author has declared that none of the authors has any competing
409 interests.

410 **Acknowledgments.** The authors would like to thank the Shenzhen National Climate Observatory
411 for providing the observation platform for this study.

412 **Financial support.** This work was supported by the National Natural Science Foundation of China
413 (42305108, 41827804), the Guangdong Provincial Observation and Research Station for Coastal
414 Atmosphere and Climate of the Greater Bay Area (2021B1212050024), the Shenzhen Science and
415 Technology Program (RCBS20221008093123058, KQTD20210811090048025,
416 KCXFZ20230731093601003), the Guangdong Basic and Applied Basic Research Foundation
417 (2023A1515011037), the Shenzhen Key Laboratory of Precision Measurement and Early Warning
418 Technology for Urban Environmental Health Risks (ZDSYS20220606100604008), the Opening
419 Project of Shanghai Key Laboratory of Atmospheric Particle Pollution and Prevention (LAP³), and
420 High Level Special Funds (G030290001).

421



References:

- Al Fischer, D., and Smith, G. D.: A portable, four-wavelength, single-cell photoacoustic spectrometer for ambient aerosol absorption, *Aerosol Sci. Technol.*, 52, 393-406, 10.1080/02786826.2017.1413231, 2018.
- Anderson, T. L., and Ogren, J. A.: Determining aerosol radiative properties using the TSI 3563 integrating nephelometer, *Aerosol Sci. Technol.*, 29, 57-69, 10.1080/02786829808965551, 1998.
- Arnott, W. P., Moosmüller, H., Rogers, C. F., Jin, T., and Bruch, R.: Photoacoustic spectrometer for measuring light absorption by aerosol: instrument description, *Atmos. Environ.*, 33, 2845-2852, 1998.
- Bianco, A., Deguillaume, L., Vaitilingom, M., Nicol, E., Baray, J. L., Chaumerliac, N., and Bridoux, M.: Molecular characterization of cloud water samples collected at the Puy de Dome (France) by fourier transform ion cyclotron resonance mass spectrometry, *Environ. Sci. Technol.*, 52, 10275-10285, 10.1021/acs.est.8b01964, 2018.
- Bond, T. C., and Bergstrom, R. W.: Light absorption by carbonaceous particles: An investigative review, *Aerosol Sci. Technol.*, 40, 27-67, 10.1080/02786820500421521, 2006.
- Bond, T. C., Covert, D. S., and Müller, T.: Truncation and angular-scattering corrections for absorbing aerosol in the TSI 3563 nephelometer, *Aerosol Sci. Technol.*, 43, 866-871, 10.1080/02786820902998373, 2009.
- Bones, D. L., Henricksen, D. K., Mang, S. A., Gonsior, M., Bateman, A. P., Nguyen, T. B., Cooper, W. J., and Nizkorodov, S. A.: Appearance of strong absorbers and fluorophores in limonene-O₃ secondary organic aerosol due to NH₄⁺-mediated chemical aging over long time scales, *J. Geophys. Res. Atmos.*, 115, 10.1029/2009jd012864, 2010.
- Cappa, C. D., Lack, D. A., Burkholder, J. B., and Ravishankara, A. R.: Bias in filter-based aerosol light absorption measurements due to organic aerosol loading: Evidence from laboratory measurements, *Aerosol Sci. Technol.*, 42, 1022-1032, 10.1080/02786820802389285, 2008.
- Chang, J. L., and Thompson, J. E.: Characterization of colored products formed during irradiation of aqueous solutions containing H₂O₂ and phenolic compounds, *Atmos. Environ.*, 44, 541-551, 10.1016/j.atmosenv.2009.10.042, 2010.
- Chen, J., Wenger, J. C., and Venables, D. S.: Near-ultraviolet absorption cross sections of nitrophenols and their potential influence on tropospheric oxidation capacity, *J. Phys. Chem. A*, 115, 12235-12242, 10.1021/jp206929r, 2011.
- Chen, Y., and Bond, T. C.: Light absorption by organic carbon from wood combustion, *Atmos. Chem. Phys.*, 10, 1773-1787, 2010.
- Claeys, M., Vermeylen, R., Yasmeen, F., Gómez-González, Y., Chi, X. G., Maenhaut, W., Mészáros,



- 456 T., and Salma, I.: Chemical characterisation of humic-like substances from urban, rural and
457 tropical biomass burning environments using liquid chromatography with UV/vis photodiode
458 array detection and electrospray ionisation mass spectrometry, *Environ. Chem.*, 9, 273-284,
459 10.1071/en11163, 2012.
- 460 Cui, M., Li, C., Chen, Y. J., Zhang, F., Li, J., Jiang, B., Mo, Y. Z., Li, J., Yan, C. Q., Zheng, M.,
461 Xie, Z. Y., Zhang, G., and Zheng, J. Y.: Molecular characterization of polar organic aerosol
462 constituents in off-road engine emissions using Fourier transform ion cyclotron resonance mass
463 spectrometry (FT-ICR MS): implications for source apportionment, *Atmos. Chem. Phys.*, 19,
464 13945-13956, 10.5194/acp-19-13945-2019, 2019.
- 465 Desyaterik, Y., Sun, Y., Shen, X. H., Lee, T. Y., Wang, X. F., Wang, T., and Collett, J. L.: Speciation
466 of "brown" carbon in cloud water impacted by agricultural biomass burning in eastern China, *J.*
467 *Geophys. Res. Atmos.*, 118, 7389-7399, 10.1002/jgrd.50561, 2013.
- 468 Feng, L., Xu, J. Z., Kang, S. C., Li, X. F., Li, Y., Jiang, B., and Shi, Q.: Chemical composition of
469 microbe-derived dissolved organic matter in cryoconite in Tibetan Plateau glaciers: Insights
470 from fourier transform ion cyclotron resonance mass spectrometry analysis, *Environ. Sci.*
471 *Technol.*, 50, 13215-13223, 10.1021/acs.est.6b03971, 2016.
- 472 Flores, J. M., Zhao, D. F., Segev, L., Schlag, P., Kiendler-Scharr, A., Fuchs, H., Watne, A. K.,
473 Bluvshstein, N., Mentel, T. F., Hallquist, M., and Rudich, Y.: Evolution of the complex refractive
474 index in the UV spectral region in ageing secondary organic aerosol, *Atmos. Chem. Phys.*, 14,
475 5793-5806, 10.5194/acp-14-5793-2014, 2014.
- 476 Gómez-González, Y., Wang, W., Vermeylen, R., Chi, X., Neirynck, J., Janssens, I. A., Maenhaut,
477 W., and Claeys, M.: Chemical characterisation of atmospheric aerosols during a 2007 summer
478 field campaign at Brasschaat, Belgium: sources and source processes of biogenic secondary
479 organic aerosol, *Atmos. Chem. Phys.*, 12, 125-138, 10.5194/acp-12-125-2012, 2012.
- 480 Haynes, J. P., Miller, K. E., and Majestic, B. J.: Investigation into photoinduced auto-oxidation of
481 polycyclic aromatic hydrocarbons resulting in brown carbon production, *Environ. Sci. Technol.*,
482 53, 682-691, 10.1021/acs.est.8b05704, 2019.
- 483 Hecobian, A., Zhang, X., Zheng, M., Frank, N., Edgerton, E., and Weber, R.: Water-soluble organic
484 aerosol material and the light-absorption characteristics of aqueous extracts measured over the
485 Southeastern United States, *Atmos. Chem. Phys.*, 10, 5965-5977, 10.5194/acp-10-5965-2010,
486 2010.
- 487 Kim, S., Kramer, R. W., and Hatcher, P. G.: Graphical method for analysis of ultrahigh-resolution
488 broadband mass spectra of natural organic matter, the van Krevelen diagram, *Anal. Chem.*, 75,
489 5336-5344, 10.1021/ac034415p, 2003.
- 490 Kitanovski, Z., Cusak, A., Grgic, I., and Claeys, M.: Chemical characterization of the main
491 products formed through aqueous-phase photonitration of guaiacol, *Atmos. Meas. Tech.*, 7,



- 492 2457-2470, 10.5194/amt-7-2457-2014, 2014.
- 493 Kourtchev, I., Fuller, S. J., Giorio, C., Healy, R. M., Wilson, E., O'Connor, I., Wenger, J. C.,
 494 McLeod, M., Aalto, J., Ruuskanen, T. M., Maenhaut, W., Jones, R., Venables, D. S., Sodeau, J.
 495 R., Kulmala, M., and Kalberer, M.: Molecular composition of biogenic secondary organic
 496 aerosols using ultrahigh-resolution mass spectrometry: comparing laboratory and field studies,
 497 *Atmos. Chem. Phys.*, 14, 2155-2167, 10.5194/acp-14-2155-2014, 2014.
- 498 Kourtchev, I., Doussin, J. F., Giorio, C., Mahon, B., Wilson, E. M., Maurin, N., Pangu, E.,
 499 Venables, D. S., Wenger, J. C., and Kalberer, M.: Molecular composition of fresh and aged
 500 secondary organic aerosol from a mixture of biogenic volatile compounds: a high-resolution
 501 mass spectrometry study, *Atmos. Chem. Phys.*, 15, 5683-5695, 10.5194/acp-15-5683-2015,
 502 2015.
- 503 Kourtchev, I., Godoi, R. H. M., Connors, S., Levine, J. G., Archibald, A. T., Godoi, A. F. L.,
 504 Paralovo, S. L., Barbosa, C. G. G., Souza, R. A. F., Manzi, A. O., Seco, R., Sjöstedt, S., Park, J.
 505 H., Guenther, A., Kim, S., Smith, J., Martin, S. T., and Kalberer, M.: Molecular composition of
 506 organic aerosols in central Amazonia: an ultra-high-resolution mass spectrometry study, *Atmos.*
 507 *Chem. Phys.*, 16, 11899-11913, 10.5194/acp-16-11899-2016, 2016.
- 508 Kristensen, K., Cui, T., Zhang, H., Gold, A., Glasius, M., and Surratt, J. D.: Dimers in α -pinene
 509 secondary organic aerosol: effect of hydroxyl radical, ozone, relative humidity and aerosol
 510 acidity, *Atmos. Chem. Phys.*, 14, 4201-4218, 10.5194/acp-14-4201-2014, 2014.
- 511 Krueve, A.: Semi-quantitative non-target analysis of water with liquid chromatography/high-
 512 resolution mass spectrometry: How far are we?, *Rapid Commun. Mass Sp.*, 33, 54-63,
 513 10.1002/rcm.8208, 2019.
- 514 Kumar, N. K., Corbin, J. C., Bruns, E. A., Massabó, D., Slowik, J. G., Drinovec, L., Mocnik, G.,
 515 Prati, P., Vlachou, A., Baltensperger, U., Gysel, M., El-Haddad, I., and Prévôt, A. S. H.:
 516 Production of particulate brown carbon during atmospheric aging of residential wood-burning
 517 emissions, *Atmos. Chem. Phys.*, 18, 17843-17861, 10.5194/acp-18-17843-2018, 2018.
- 518 Lack, D. A., Cappa, C. D., Covert, D. S., Baynard, T., Massoli, P., Sierau, B., Bates, T. S., Quinn,
 519 P. K., Lovejoy, E. R., and Ravishankara, A. R.: Bias in filter-based aerosol light absorption
 520 measurements due to organic aerosol loading: Evidence from ambient measurements, *Aerosol*
 521 *Sci. Technol.*, 42, 1033-1041, 10.1080/02786820802389277, 2008.
- 522 Lambe, A. T., Cappa, C. D., Massoli, P., Onasch, T. B., Forestieri, S. D., Martin, A. T., Cummings,
 523 M. J., Croasdale, D. R., Brune, W. H., Worsnop, D. R., and Davidovits, P.: Relationship between
 524 oxidation level and optical properties of secondary organic aerosol, *Environ. Sci. Technol.*, 47,
 525 6349-6357, 10.1021/es401043j, 2013.
- 526 Laskin, A., Laskin, J., and Nizkorodov, S. A.: Chemistry of atmospheric brown carbon, *Chem.*
 527 *Rev.*, 10.1021/cr5006167, 2015.



- 528 Lewis, K., Arnott, W. P., Moosmuller, H., and Wold, C. E.: Strong spectral variation of biomass
 529 smoke light absorption and single scattering albedo observed with a novel dual-wavelength
 530 photoacoustic instrument, *J. Geophys. Res. Atmos.*, 113, 10.1029/2007jd009699, 2008.
- 531 Li, C. L., He, Q. F., Hettiyadura, A. P. S., Käfer, U., Shmul, G., Meidan, D., Zimmermann, R.,
 532 Brown, S. S., George, C., Laskin, A., and Rudich, Y.: Formation of secondary brown carbon in
 533 biomass burning aerosol proxies through NO₃ radical reactions, *Environ. Sci. Technol.*, 54,
 534 1395-1405, 10.1021/acs.est.9b05641, 2020.
- 535 Li, K., Wang, W. G., Ge, M. F., Li, J. J., and Wang, D.: Optical properties of secondary organic
 536 aerosols generated by photooxidation of aromatic hydrocarbons, *Sci. Rep.*, 4,
 537 10.1038/srep04922, 2014.
- 538 Massabò, D., Caponi, L., Bove, M. C., and Prati, P.: Brown carbon and thermal-optical analysis:
 539 A correction based on optical multi-wavelength apportionment of atmospheric aerosols, *Atmos.*
 540 *Environ.*, 125, 119-125, 10.1016/j.atmosenv.2015.11.011, 2016.
- 541 Massoli, P., Kebabian, P. L., Onasch, T. B., Hills, F. B., and Freedman, A.: Aerosol light extinction
 542 measurements by cavity attenuated phase shift (CAPS) spectroscopy: Laboratory validation and
 543 field deployment of a compact aerosol particle extinction monitor, *Aerosol Sci. Technol.*, 44,
 544 428-435, 10.1080/02786821003716599, 2010.
- 545 Moise, T., Flores, J. M., and Rudich, Y.: Optical properties of secondary organic aerosols and their
 546 changes by chemical processes, *Chem. Rev.*, 10.1021/cr5005259, 2015.
- 547 Nozière, B., Dziedzic, P., and Córdova, A.: Products and kinetics of the liquid-phase reaction of
 548 glyoxal catalyzed by ammonium ions (NH₄⁺), *J. Phys. Chem. A*, 113, 231-237,
 549 10.1021/jp8078293, 2009.
- 550 Ohno, T., He, Z. Q., Sleighter, R. L., Honeycutt, C. W., and Hatcher, P. G.: Ultrahigh resolution
 551 mass spectrometry and indicator species analysis to identify marker components of soil- and
 552 plant biomass-derived organic matter fractions, *Environ. Sci. Technol.*, 44, 8594-8600,
 553 10.1021/es101089t, 2010.
- 554 Olson, M. R., Garcia, M. V., Robinson, M. A., Van Rooy, P., Dietenberger, M. A., Bergin, M., and
 555 Schauer, J. J.: Investigation of black and brown carbon multiple-wavelength-dependent light
 556 absorption from biomass and fossil fuel combustion source emissions, *J. Geophys. Res. Atmos.*,
 557 120, 6682-6697, 10.1002/2014jd022970, 2015.
- 558 Pani, S. K., Lin, N. H., Griffith, S. M., Chantara, S., Lee, C. T., Thepnuan, D., and Tsai, Y.: Brown
 559 carbon light absorption over an urban environment in northern peninsular Southeast Asia,
 560 *Environ. Pollut.*, 276, 10.1016/j.envpol.2021.116735, 2021.
- 561 Petzold, A., Schloesser, H., Sheridan, P. J., Arnott, W. P., Ogren, J. A., and Virkkula, A.: Evaluation
 562 of multiangle absorption photometry for measuring aerosol light absorption, *Aerosol Sci.*
 563 *Technol.*, 39, 40-51, 10.1080/027868290901945, 2005.



- 564 Rathod, T. D., Sahu, S. K., Tiwari, M., Bhangare, R. C., and Ajmal, P. Y.: Optical properties of
 565 water soluble and organic soluble carbonaceous aerosols at an urban location in India, *Atmos.*
 566 *Pollut. Res.*, 15, 10.1016/j.apr.2023.101956, 2024.
- 567 Riziq, A. A., Erlick, C., Dinar, E., and Rudich, Y.: Optical properties of absorbing and non-
 568 absorbing aerosols retrieved by cavity ring down (CRD) spectroscopy, *Atmos. Chem. Phys.*, 7,
 569 1523-1536, 2007.
- 570 Saleh, R., Robinson, E. S., Tkacik, D. S., Ahern, A. T., Liu, S., Aiken, A. C., Sullivan, R. C., Presto,
 571 A. A., Dubey, M. K., Yokelson, R. J., Donahue, N. M., and Robinson, A. L.: Brownness of
 572 organics in aerosols from biomass burning linked to their black carbon content, *Nat. Geosci.*, 7,
 573 647-650, 10.1038/ngeo2220, 2014.
- 574 Saleh, R., Cheng, Z. Z., and Atwi, K.: The brown-black continuum of light-absorbing combustion
 575 aerosols, *Environ. Sci. Technol. Lett.*, 5, 508-513, 10.1021/acs.estlett.8b00305, 2018.
- 576 Saleh, R.: From measurements to models: Toward accurate representation of brown carbon in
 577 climate calculations, *Curr. Pollut. Rep.*, 6, 90-104, 10.1007/s40726-020-00139-3, 2020.
- 578 Shapiro, E. L., Szprengiel, J., Sareen, N., Jen, C. N., Giordano, M. R., and McNeill, V. F.: Light-
 579 absorbing secondary organic material formed by glyoxal in aqueous aerosol mimics, *Atmos.*
 580 *Chem. Phys.*, 9, 2289-2300, 10.5194/acp-9-2289-2009, 2009.
- 581 Shetty, N. J., Pandey, A., Baker, S., Hao, W. M., and Chakrabarty, R. K.: Measuring light
 582 absorption by freshly emitted organic aerosols: optical artifacts in traditional solvent-extraction-
 583 based methods, *Atmos. Chem. Phys.*, 19, 8817-8830, 10.5194/acp-19-8817-2019, 2019.
- 584 Song, J. Z., Li, M. J., Jiang, B., Wei, S. Y., Fan, X. J., and Peng, P. A.: Molecular characterization
 585 of water-soluble humic like substances in smoke particles emitted from combustion of biomass
 586 materials and coal using ultrahigh-resolution electrospray ionization fourier transform ion
 587 cyclotron resonance mass spectrometry, *Environ. Sci. Technol.*, 52, 2575-2585,
 588 10.1021/acs.est.7b06126, 2018.
- 589 Song, J. Z., Li, M. J., Fan, X. J., Zou, C. L., Zhu, M. B., Jiang, B., Yu, Z. Q., Jia, W. L., Liao, Y.
 590 H., and Peng, P. A.: Molecular characterization of water- and methanol-soluble organic
 591 compounds emitted from residential coal combustion using ultrahigh-resolution electrospray
 592 ionization fourier transform ion cyclotron resonance mass spectrometry, *Environ. Sci. Technol.*,
 593 53, 13607-13617, 10.1021/acs.est.9b04331, 2019.
- 594 Subramanian, R., Roden, C. A., Boparai, P., and Bond, T. C.: Yellow beads and missing particles:
 595 Trouble ahead for filter-based absorption measurements, *Aerosol Sci. Technol.*, 41, 630-637,
 596 10.1080/02786820701344589, 2007.
- 597 Sumlin, B. J., Pandey, A., Walker, M. J., Pattison, R. S., Williams, B. J., and Chakrabarty, R. K.:
 598 Atmospheric photooxidation diminishes light absorption by primary brown carbon aerosol from
 599 biomass burning, *Environ. Sci. Technol. Lett.*, 4, 540-545, 10.1021/acs.estlett.7b00393, 2017.



- 600 Sun, H., Biedermann, L., and Bond, T. C.: Color of brown carbon: A model for ultraviolet and
 601 visible light absorption by organic carbon aerosol, *Geophys. Res. Lett.*, 34,
 602 10.1029/2007gl029797, 2007.
- 603 Tao, S., Lu, X., Levac, N., Bateman, A. P., Nguyen, T. B., Bones, D. L., Nizkorodov, S. A., Laskin,
 604 J., Laskin, A., and Yang, X.: Molecular characterization of organosulfates in organic aerosols
 605 from Shanghai and Los Angeles urban areas by nanospray-desorption electrospray ionization
 606 high-resolution mass spectrometry, *Environ. Sci. Technol.*, 48, 10993-11001,
 607 10.1021/es5024674, 2014.
- 608 Updyke, K. M., Nguyen, T. B., and Nizkorodov, S. A.: Formation of brown carbon via reactions
 609 of ammonia with secondary organic aerosols from biogenic and anthropogenic precursors,
 610 *Atmos. Environ.*, 63, 22-31, 10.1016/j.atmosenv.2012.09.012, 2012.
- 611 Wen, H., Zhou, Y., Xu, X., Wang, T., Chen, Q., Chen, Q., Li, W., Wang, Z., Huang, Z., Zhou, T.,
 612 Shi, J., Bi, J., Ji, M., and Wang, X.: Water-soluble brown carbon in atmospheric aerosols along
 613 the transport pathway of Asian dust: Optical properties, chemical compositions, and potential
 614 sources, *Sci. Total Environ.*, 789, 10.1016/j.scitotenv.2021.147971, 2021.
- 615 Wong, J. P. S., Nenes, A., and Weber, R. J.: Changes in light absorptivity of molecular weight
 616 separated brown carbon due to photolytic aging, *Environ. Sci. Technol.*, 51, 8414-8421,
 617 10.1021/acs.est.7b01739, 2017.
- 618 Zarzana, K. J., De Haan, D. O., Freedman, M. A., Hasenkopf, C. A., and Tolbert, M. A.: Optical
 619 properties of the products of α -dicarbonyl and amine reactions in simulated cloud droplets,
 620 *Environ. Sci. Technol.*, 46, 4845-4851, 10.1021/es2040152, 2012.
- 621 Zeng, Y. L., Zhang, A. T., Yang, X., Xing, C. B., Zhai, J. H., Wang, Y. X., Cai, B. H., Shi, S., Zhang,
 622 Y. J., Shen, Z. X., Fu, T. M., Zhu, L., Shen, H. Z., Ye, J. H., and Wang, C.: Internal exposure
 623 potential of water-soluble organic molecules in urban PM_{2.5} evaluated by non-covalent
 624 adductome of human serum albumin, *Environ. Int.*, 184, 10.1016/j.envint.2024.108492, 2024.
- 625 Zhai, J., Wang, X., Li, J., Xu, T., Chen, H., Yang, X., and Chen, J.: Thermal desorption single
 626 particle mass spectrometry of ambient aerosol in Shanghai, *Atmos. Environ.*, 123, 407-414,
 627 10.1016/j.atmosenv.2015.09.001, 2015.
- 628 Zhang, A. T., Zeng, Y. L., Yang, X., Zhai, J. H., Wang, Y. X., Xing, C. B., Cai, B. H., Shi, S., Zhang,
 629 Y. J., Shen, Z. X., Fu, T. M., Zhu, L., Shen, H. Z., Ye, J. H., and Wang, C.: Organic matrix effect
 630 on the molecular light absorption of brown carbon, *Geophys. Res. Lett.*, 50,
 631 10.1029/2023gl106541, 2023.
- 632 Zhang, X. L., Lin, Y. H., Surratt, J. D., and Weber, R. J.: Sources, composition and absorption
 633 angstrom exponent of light-absorbing organic components in aerosol extracts from the Los
 634 Angeles Basin, *Environ. Sci. Technol.*, 47, 3685-3693, 10.1021/es305047b, 2013.
- 635 Zhong, M., and Jang, M.: Light absorption coefficient measurement of SOA using a UV-Visible



636 spectrometer connected with an integrating sphere, Atmos. Environ., 45, 4263-4271,
637 10.1016/j.atmosenv.2011.04.082, 2011.